

The Heart-shaped Supernova Remnant 3C 391 viewed in Multi-bands

Yang Su, Yang Chen

Department of Astronomy, Nanjing University, Nanjing 210093, P.R. China

Abstract

Using *Chandra* X-ray, *Spitzer* mid-IR, and 1.5 GHz radio data, we examine the spatial structure of SNR 3C 391. The X-ray surface brightness is generally anti-correlative with the IR and radio brightness. The multiband data clearly exhibit a heart-shaped morphology and show the multi-shell structure of the remnant. A thin brace-like shell on the south detected at 24 μ m is projected outside the radio border and confines the southern faint X-ray emission. The leading 24 μ m knot on the SE boundary appears to be partly surrounded by soft X-ray emitting gas. The mid-IR emission is dominated by the contribution of the shocked dust grains, which may have been partly destroyed by sputtering.

Key words: ISM, Supernova remnants, 3C 391 (G31.9+0.0), X-rays, Infrared, Dust

1 Introduction

Galactic molecular clouds, containing about half the mass of the interstellar medium (ISM), have a complex structure, and stars form out of the densest regions therein. Massive stars have often not moved far from their birthsites by the time they explode as a core-collapse supernova, and therefore the interaction of supernova remnants (SNRs) with molecular clouds can plausibly occur. The number of SNRs with convincing evidence for interaction with ambient molecular clouds is about 20, and a large fraction of them are mixed-morphology or thermal composite SNRs, with interior-filled thermal X-ray emission surrounded by a radio shell (Yusef-Zadeh et al., 2003).

When SNRs interact with inhomogeneous molecular gas with a large density variation, the morphology and structure is not expected to be regular or symmetric. Features such as gas clumps, incomplete arcs, blowout shells, thin or thick filaments, etc., can typically be observed in radio, infrared (IR), optical,

or X-rays. SNR 3C 391 is one of the prototype mixed-morphology or thermal composite SNRs, confirmed to be interacting with molecular clouds to the northwest (Rho & Peter, 1998; Wilner et al., 1998; Reach & Rho, 1999; Chen & Slane, 2001). Due to its remarkable radio shell elongated from northwest (NW) to southeast (SE), it is suggested to have broken out of a dense region into an adjacent region of low density (Reynolds & Moffett, 1993). The bright clumpy thermal X-ray emission arises from the remnant interior, and the rim is X-ray faint (Chen & Slane, 2001; Chen et al., 2004, hereafter CSSW04). The *Spitzer Space Telescope (SST)* (Werner et al., 2004) *Infrared Array Camera (IRAC)* near-IR observations show a bright incomplete shell correlated well with the NW radio structure which is tangent to a giant molecular cloud (Reach et al., 2005; Lee, 2005). These structure patterns at different wavelengths show complex physical conditions in SNR 3C 391, and reflect inhomogeneities in the ISM.

Here we will show an overall view of SNR 3C 391 combining the radio (1.5 GHz), mid-IR (*SST* 24 & 70 μ m), and X-ray (*Chandra*) observations, and examine the spatial structures in different wavelengths.

2 Multi-band observation of 3C 391

2.1 The Radio and X-ray Morphology

In the radio images (Reynolds & Moffett, 1993; Moffett & Reynolds, 1994), 3C 391 has a bright partial shell along the north and NW boundary. The NW part of the remnant appears to be a broken bubble, with the brightest radio bar along the western border and a faint blowout extending to the SE. Two 1720 MHz OH maser spots are detected along the radio shell (Frail et al., 1996). Reynolds & Moffett (1993) suggest that the remnant may have resulted from a supernova explosion in the interior of the molecular cloud and is expanding into a region of greatly varying density.

The *Einstein* (Wang & Seward, 1984) and *ROSAT* (Rho & Peter, 1996) X-ray observations show a strong soft X-ray emission arising from the southeast region of the remnant. Both the *ASCA* and *Chandra* observations show a SE-NW elongated broad-band X-ray morphology, similar to the radio image (Chen & Slane, 2001; CSSW04). The X-ray emission peaks southeast of the geometric center of the radio pattern. The X-ray emission from the interior to the NW bubble suffers higher absorption than that from the SE blowout part. The *Chandra* observation reveals rich small-scale structures, such as knots and arcs, as well as faint, diffuse gas that appears to expand out of the southwestern radio boundary (CSSW04). In the southwest (SW), the narrow

band analysis of the S and Si X-ray lines unveils a very faint jet-like protrusion projected outside the radio border (Su & Chen, 2005).

To better show the entire spatial X-ray emitting remnant, we rebin the cleaned level 2 *Chandra* data (ObsID 2786; CSSW04) using an adaptive mesh to include at least 9 counts (0.3-7 keV) per bin. The contours of the rebinned image are plotted in Fig. 1a. In this figure, a broad band X-ray protrusion (corresponding to the narrow band one) is seen in the SW.

2.2 Mid-IR images

The mid-IR 24 μm and 70 μm observations used here were carried out as part of the 24 and 70 Micron Survey of the Inner Galactic Disk Program (PID: 20597, PI: Sean Carey) with the Multiband Imaging Photometer (MIPS) (Rieke et al., 2004). The data are obtained from *Spitzer* archive. The raw 24 μm image of 3C 391 from the Post Basic Calibrated Data is shown in Fig. 1b, which displays the remnant extent which is similar to that seen in radio and X-rays. We sum 24296 pixels (~ 3.7 arcmin radius) to get the total surface brightness and select faint regions outside the SNR as the background. Subtracting the mean surrounding IR background $\sim 60 \pm 3$ MJy/sr, we obtain a mean surface brightness of 3C 391 $\sim 11.5 \pm 3.0$ MJy/sr or a flux $\sim 37.9 \pm 9.9$ Jy. After a manual subtraction of nearby emission features, the remaining 24 μm emission is superposed on the X-ray contours in Fig. 1a. The manually subtracted 24 μm and 70 μm emission maps are overlaid with the 1.5 GHz radio contours in Fig. 2. Tricolor image with 1.5 GHz radio emission in red, 24 μm IR emission in green, and 0.3–7.0 keV X-rays in blue is shown in Fig. 3. In the 70 μm mid-IR image there are some streaks mixed with the IR emission and it is very difficult to determine the background intensity or the pure mid-IR intensity associated with SNR. We use the GeRT package (<http://ssc.spitzer.caltech.edu/mips/gert>) and the software tool MOPEX (<http://ssc.spitzer.caltech.edu/postbcd/download-mopex.html>) to create a new mosaic of 70 μm . After running MOPEX on the filtered Basic Calibrated Data (BCD) images produced by the data processing pipeline, some arc-like structures of 3C 391 are visible in 70 μm (Fig. 2b).

The two mid-IR images (Fig. 2) display several thick arc-like structures along the SW, NW, and northeast (NE) boundaries. A very faint 24 μm brace-symbol-like thin arc structure in the south is projected outside the radio border and goes from west to south along the edge of the faint X-ray emission.

In the 24 μm emission map (Fig. 1a, 1b), there are two bright knots at $(18^{\text{h}}49^{\text{m}}39^{\text{s}}.9, -00^{\circ}56'40'')$ and $(18^{\text{h}}49^{\text{m}}39^{\text{s}}.4, -00^{\circ}58'36'')$ on the east and southeast border, respectively. They seem to correspond to X-ray knots (Fig. 3).

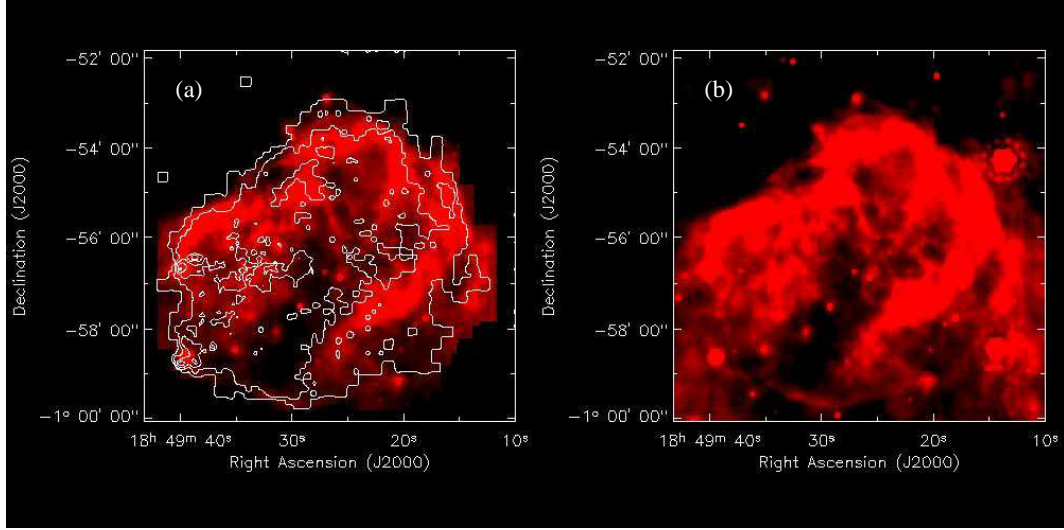


Fig. 1. (a) Superposition of *Chandra* X-ray (0.3-7.0 keV) contours of 3C 391 on the MIPS 24 μ m image. The X-ray contours are between the 5% maximum and the 90% maximum with a square-root scale. The IR intensity range is from 62 MJy sr^{-1} to 80 MJy sr^{-1} , with a linear transfer function and the point-like IR sources away from the SNR have been removed. (b) The SST MIPS 24 μ m raw image of SNR 3C 391. The IR intensity range is from 58 MJy sr^{-1} to 92 MJy sr^{-1} , with a linear transfer function but the background and the point-like sources have not been removed.

The east knot is the 24 μ m counterpart of IR source IRAS 18470–0100 (CSSW04), with improved positional resolution. It can also be seen that a line of point-like IR sources are evenly spaced extending from the remnant center to the bright SE knot. These five sources have 2MASS near-IR counterparts with accurate positions: (18^h49^m27^s.17, $-00^{\circ}56'44''$.1), (18^h49^m29^s.34, $-00^{\circ}57'29''$.9), (18^h49^m31^s.43, $-00^{\circ}58'02''$.5), (18^h49^m35^s.15, $-00^{\circ}58'26''$.1), and (18^h49^m39^s.50, $-00^{\circ}58'36''$.0). The IR source at the geometric center has an X-ray counterpart (CXJ 184927.0-005640; CSSW04) given $\sim 4''$ spatial resolution of 2MASS. The nature of these sources is interesting but unknown yet. If the central one suffers an interstellar absorption similar to that of 3C 391 ($N_H \sim 3 \times 10^{22} \text{ cm}^{-2}$), assuming its X-ray spectrum as a thermal plasma with a temperature of 0.6 keV (for soft case) and 2 keV (for hard case), respectively, typical for normal early-type stars, we estimate the 0.3 – 8 keV luminosity of the X-ray source as $\sim 4.3 \times 10^{32} \text{ ergs s}^{-1}$ (for soft case) and $\sim 3.3 \times 10^{33} \text{ ergs s}^{-1}$ (for hard case) based on the X-ray count rates (Table 1 in CSSW04). It indicates that, on this assumption, the central source would most probably represent an individual early-type star or even a massive colliding stellar wind binary.

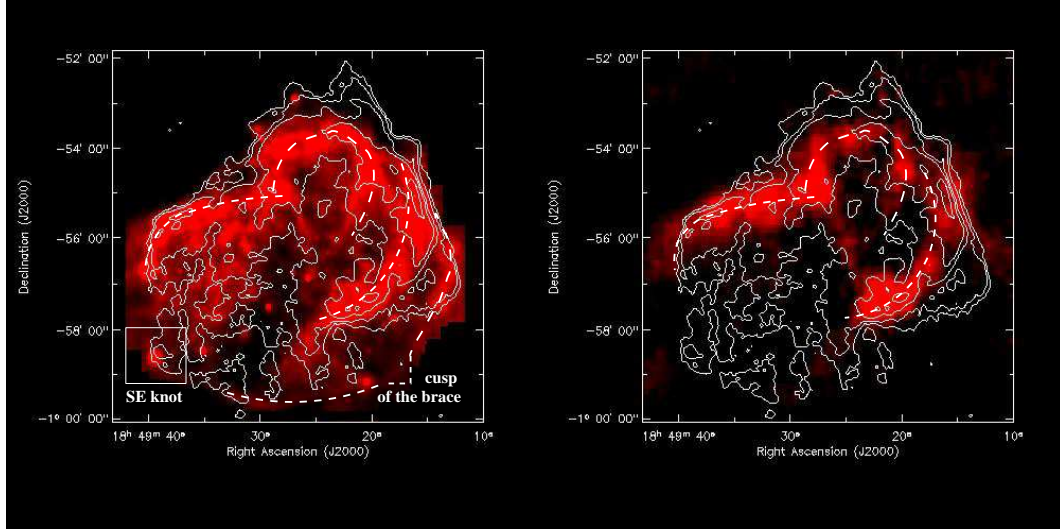


Fig. 2. (a) The SST MIPS 24 μm image of SNR 3C 391, overlaid with the 1.5 GHz radio contours. The IR intensity range is from 62 MJy sr^{-1} to 80 MJy sr^{-1} , with a linear transfer function and the point-like IR sources away the SNR are removed. The overlaid 1.5 GHz radio contours are at 1.5, 3.19, 8.25, 16.69, 43.68, and 62.24×10^{-3} Jy/beam (from Moffett & Reynolds 1994). (b) The MIPS 70 μm image of SNR 3C 391 overlaid with the same radio contours as used in (a). The radio character of the image is same as in (a). The dashed lines indicate pronounced IR arc/shell-like structures.

3 Discussion

3.1 Spatial comparison among X-ray, mid-IR, and radio emissions

Using the available radio, IR, and X-ray data, we can investigate the structure of SNR 3C 391. Seen in the tricolor image (Fig. 3), the X-ray surface brightness is generally anti-correlative with the IR and radio brightness, or anti-correlative with the environmental density because of intervening extinction. In the NW half of the remnant, two distinct thick arc-like structures in both 24 and 70 μm coincide grossly with the radio shell (Fig. 2 and Fig. 3). The westernmost bar-like radio peak and the “broad molecular line” (BML) region are located along the west-southwest IR shell, which represents a dense shocked region. The two 1720 MHz OH maser spots (Frail et al., 1996) are harbored in the NE and SW thick radio/mid-IR shells. On the NE boundary, a thick mid-IR arc is coincident with the radio shell, too. These arcs/shells are also discernible in the *SST* 5.8 μm near-IR images (Reach et al., 2005; Lee, 2005).

Apart from the above general comparison, we note two features of particular interest.

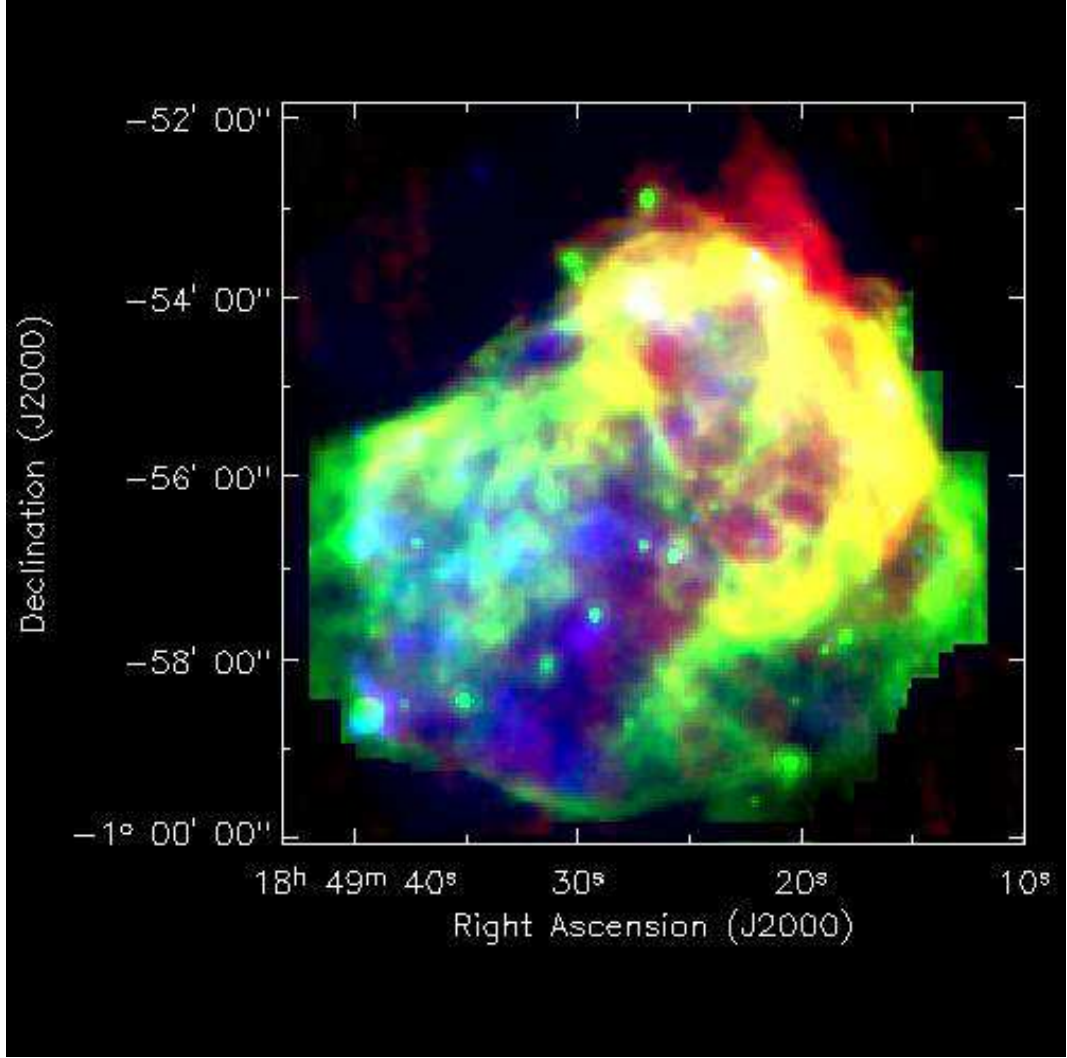


Fig. 3. Tricolor image of SNR 3C 391. The 1.5 GHz radio is coded in red, the *SST* 24 μ m IR in green, and the *Chandra* X-ray in blue. The intensity map is square-root scaled in each energy band.

1. The knot on the southeastern border ($18^{\text{h}}49^{\text{m}}39^{\text{s}}.4$, $-00^{\circ}58'36''$) (the SE knot in Fig. 2a) appears to be partly surrounded by soft X-rays (Fig. 4). Two possible mechanisms may explain this small-scale phenomenon. First, after the blast strikes a small dense cloud, a transmitted shock heats the cloud to emit 24 μ m emission, while a bow-like reflected shock stands around the cloud (McKee & Cowie, 1975). Second, after the cloud is shocked by the blast wave, materials are evaporated from the cloud and form a soft X-ray emitting gas layer (Cowie & McKee, 1977).
2. The 24 μ m brace-like thin shell (Fig. 2a) appears to be projected outside the long southern radio border of the remnant (Fig. 2a and Fig. 3). It has not been seen before at any wavelengths. However, it confines very well the faint X-ray emitting emission that fades out from the remnant interior and seems to

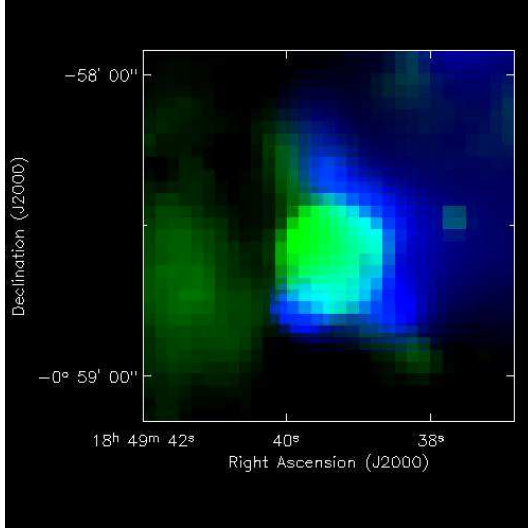


Fig. 4. The southeastern boundary region. The $24 \mu\text{m}$ IR emission is coded in green, and the *Chandra* soft (0.3-2.6 keV) X-ray emission in blue.

extend beyond the SW radio border (CSSW04) (Fig. 1a and Fig. 3). Moreover, the position of the cusp of the “brace” (Fig. 2a) is coincident with a jet-like protrusion seen in the narrow band X-ray maps for S and Si (Su & Chen, 2005). Such positional consistency between the $24 \mu\text{m}$ and X-ray emission suggests that the thin brace-like IR shell is associated with the remnant. Thus, the 3C 391 SNR has a larger volume than previously recognized and takes a heart-like shape with combination of the X-ray, IR, and radio emission (Fig. 2a and Fig. 3). The multi-shells, especially the newly detected southern thin shell, indicate that the molecular clouds around this remnant are distributed more complexly than previously assumed. The NW clouds have a non-uniform structure and there is a low density region in the south, into which a part of the supernova blast wave propagates.

3.2 The $24 \mu\text{m}$ mid-IR emission of the multi-shells

The $24 \mu\text{m}$ emission more distinctly demonstrates shell structures of SNR 3C 391 than other IR wavelength emission. Similar phenomena occur in some other SNRs (Stanimirovic et al., 2005; Morris et al., 2006; Borkowski et al., 2006). Hence the $24 \mu\text{m}$ band seems to be an effective window for SNR observation. The near-IR emission from various portions of the 3C 391 SNR has been suggested to be dominated by atomic fine-structure lines and synchrotron emission (from electrons in the moderate-density molecular regions) or molecular lines and ionic lines (from the high density molecular gas) (Reach et al., 2005). Here we suggest that the mid-IR emission of 3C 391 mainly arises from dust grains.

The origin of the 24 μm mid-IR emission is not clear. We explored possible mechanisms of synchrotron, atomic lines, molecular lines, or IR emission from shock-heated dust grains. Let us compare the contribution of each mechanism to the 24 μm emission of 3C 391. (a) *Synchrotron*. Using the integrated flux at 330 MHz of 41.0 Jy and the spectral index $\sim -0.49 \pm 0.1$ (Brogan et al. 2005), we estimate the flux by extrapolation to be less than 0.3 Jy (1% total) at 24 μm . Certainly, the mid-IR emission of the brace-like thin shell is not synchrotron, otherwise it should have been discernible at 70 μm . (b) *Ionic lines*. The SST MIPS band at 24 μm contains ionic lines of [FeII] at 25.988 μm and [OIV] at 25.890 μm (Reach & Rho, 2000). In the BML region and the radio bar-like peak, the [FeII] plus [OIV] lines amount to no more than 40% and 30% of the local MIPS IR 24 μm fluxes, respectively (Reach & Rho, 2000). We assume that similar fractions hold for the entire remnant but note that this may overestimate the fraction because the two regions are the brightest in the ionic lines. (c) *Molecular lines*. Some rotational molecular lines such as from OH and H₂O may contribute to the mid-IR emission, but generally mid-IR from molecular lines is weak compared with the strong continuum emission of dust grains (Gorti & Hollenbach, 2004). Also, the ISO observations of this remnant do not show strong molecular lines at 24 μm (e.g., Reach & Rho, 2000). (d) *Dust emission*. Since the 24 μm emission of 3C 391 is not dominated by any of the above three mechanisms, we suggest that it predominantly ($> 60\%$) originates from dust grains. The concentration of the 24 μm emission on the remnant shells also favors that the dust in SNR 3C 391 is part of the swept-up, shock-heated ISM. This physics of explanation is similar to that for the mid-IR emission of SNR N132D (Tappe et al., 2006).

The blackbody temperature of the dust grains in SNR 3C 391 was estimated as 140 K for 12-24 μm and 52 K for 24-100 μm from the *IRAS* observation (Arendt 1989). The total mass M_d of the hot dust associated with the SNR at temperature T_d is given by:

$$M_d = \frac{d^2 F_\nu(\lambda)}{\kappa(\lambda) B_\nu(\lambda, T_d)} , \quad (1)$$

where $F_\nu(\lambda)$ is the observed 24 μm flux ($\gtrsim 23$ Jy), $d \sim 8.0$ kpc the distance to the remnant (Chen & Slane 2001), $\kappa_\lambda = 2.5(\lambda/450\mu\text{m})^{-2.0}$ cm² g⁻¹ the dust mass absorption coefficient (Draine & Lee 1984), and $B_\nu(\lambda, T_d)$ the Planck function evaluated at the dust temperature. Thus we get a lower limit on the dust mass $M_d \gtrsim 2 \times 10^{-4} M_\odot$ for $T_d \sim 140$ K and $M_d \gtrsim 0.3 M_\odot$ for $T_d \sim 52$ K. With the mass of the X-ray emitting gas of the remnant $M_g \sim 100 M_\odot$ (CSSW04), the dust-to-gas mass ratio is then $\gtrsim 2 \times 10^{-6}$ – 3×10^{-3} (for 60% infrared flux accounted) and $\lesssim 3 \times 10^{-6}$ – 5×10^{-3} (for 100% infrared flux accounted). The estimated ratio is smaller than the normal Galactic value (~ 0.01 ; Spitzer, 1978), implying that a fraction of the shocked dust grains have been destroyed by sputtering. Given the lifetime of the dust grains destroyed

by sputtering for gas temperature $\gtrsim 10^6$ K, $\tau_{\text{sput}} \approx 10^6 a(\mu\text{m})/n(\text{cm}^{-3})$ yr (where a is the grain radius; Dwek & Werner 1981), and adopting the gas density $n \sim 2 \text{ cm}^{-3}$ for the 3C 391 (CSSW04), we could essentially expect that some large grains ($a \gtrsim 0.01 \mu\text{m}$) which were initially present survive for the age of the remnant ($\sim 4 \times 10^3$ yr) (CSSW04).

4 Summary

We have compared the morphology of SNR 3C 391 with the data of *Chandra* X-ray, *SST* mid-IR, and 1.5 GHz radio observations. The X-ray surface brightness is generally anti-correlative with the IR and radio brightness. The combination of the three band data clearly exhibits an multi-shell structure and a heart-shaped entire morphology for the remnant. Some detailed structures are revealed:

1. A thin brace-like shell detected at $24 \mu\text{m}$, which is projected outside the radio border confines the southern faint X-ray emission. The cusp is coincident with sn X-ray protrusion.
2. The $24 \mu\text{m}$ knot on the SE boundary appears to be partly surrounded by soft X-rays.

The mid-IR emission is probably dominated by dust grains, which are heated by the shocked hot gas and may have been partly destroyed by sputtering.

Acknowledgements: We have benefited from the archived *Spitzer* 24 and 70 Micron Survey of the Inner Galactic Disk Program. Two anonymous referees are thanked for useful comments that led to various improvements in the presentation of this paper. Y.C. acknowledges support from NSFC grants 10221001 and 10673003.

References

Arendt, R. G. 1989. An infrared survey of Galactic supernova remnants. *Astrophysical Journal Supplement Series* 70, 181-212.

Borkowski, K. J., Williams, B. J., Reynolds, S. P., Blair, W. P., Ghavamian, P., Sankrit, R., Hendrick, S. P., Long, K. S., Raymond, J. C., Smith, R. C., Points, S., Winkler, P. F. 2006. Dust Destruction in Type Ia Supernova Remnants in the Large Magellanic Cloud. *Astrophysical Journal* 642, L141-L144.

Brogan, C. L., Lazio, T. J., Kassim, N. E., & Dyer, K. K. 2005. Spatially Resolved Low-Frequency Very Large Array Observations of the Supernova Remnant 3C 391. *Astronomical Journal* 130, 148-155.

Chen, Y., & Slane, P. O. 2001. ASCA Observations of the Thermal Composite Supernova Remnant 3C 391. *Astrophysical Journal* 563, 202-208.

Chen, Y., Su, Y., Slane, P. O., & Wang, Q. D. 2004. A *Chandra* ACIS View of the Thermal Composite Supernova Remnant 3C 391. *Astrophysical Journal* 616, 885-894.

Cowie, L. L. & McKee, C. F. 1977. The evaporation of spherical clouds in a hot gas. I – Classical and saturated mass loss rates. *Astrophysical Journal* 211, 135-146.

Draine, B. T., & Lee, H. M. 1984. Optical properties of interstellar graphite and silicate grains. *Astrophysical Journal* 285, 89-108.

Dwek, E. & Werner, M. W. 1981. The infrared emission from supernova condensates. *Astrophysical Journal* 248, 138-151.

Frail, D. A., Goss, W. M., Reynoso, E. M., Giacani, E. B., Green, A. J., Otrupcek, R. 1996. A Survey for OH(1720 MHz) Maser Emission Toward Supernova Remnants. *Astronomical Journal* 111, 1651-1659.

Gorti, U., & Hollenbach, D. J. 2004. Models of Chemistry, Thermal Balance, and Infrared Spectra from Intermediate-Aged Disks around G and K Stars. *Astrophysical Journal* 613, 424-447.

Lee, H. G. 2005. Infrared Supernova Remnants in the *Spitzer* Glimpse Field. *Journal of the Korean Astronomical Society* 38, 385-414.

McKee, C. F. & Cowie, L. L. 1975. The interaction between the blast wave of a supernova remnant and interstellar clouds. *Astrophysical Journal* 195, 715-725.

Moffett, A. A., & Reynolds, S. P. 1994. Multifrequency studies of bright radio supernova remnants. 1: 3C 391. *Astrophysical Journal* 425, 668-686.

Morris, P. W., Stolovy, S., Wachter, S., Noriega-Crespo, A., Pannuti, T. G., Hoard, D. W. 2006. Tentative Discovery of a New Supernova Remnant in Cepheus: Unveiling an Elusive Shell in the *Spitzer* Galactic First Look Survey. *Astrophysical Journal* 640, L179-L182.

Reach, W. T., & Rho, J. H. 1999. Excitation and Disruption of a Giant Molecular Cloud by the Supernova Remnant 3C 391. *Astrophysical Journal* 511, 836-846.

Reach, W. T., & Rho, J. H. 2000. Infrared Spectroscopy of Molecular Supernova Remnants. *Astrophysical Journal* 544, 843-858.

Reach, W. T., Rho, J. H., Tappe, A., Pannuti, T. G., Brogan, C. L., Churchwell, E. B., Meade, M. R., Babler, B., Indebetouw, R., Whitney, B. A. 2005. A *Spitzer* Space Telescope Infrared Survey of Supernova Remnants in the Inner Galaxy. *Astronomical Journal* 131, 1479-1500.

Reynolds, S. P., & Moffett, D. A. 1993. High-resolution radio observations of the supernova remnant 3C 391 - Possible breakout morphology. *Astronomical Journal* 105, 2226-2230.

Rho, J. H., & Peter, R. 1996. *ROSAT* PSPC Observation of the Supernova Remnant 3C 391. *Astrophysical Journal* 467, 698.

Rho, J. H., & Peter, R. 1998. Mixed-Morphology Supernova Remnants. *Astrophysical Journal* 503, L167-170.

Rieke, G. H., Young, E. T., Engelbracht, C. W., Kelly, D. M., Low, F. J., Haller, E. E., Beeman, J. W., Gordon, K. D., Stansberry, J. A., Misselt, K. A., Cadien, J., Morrison, J. E., Rivlis, G., Latter, W. B., Noriega-Crespo, A., Padgett, D. L., Stapelfeldt, K. R., Hines, D. C., Egami, E., Muzerolle, J., Alonso-Herrero, A., Blaylock, M., Dole, H., Hinz, J. L., Le Floc'h, E., Papovich, C., Prez-Gonzlez, P. G., Smith, P. S., Su, K. Y. L., Bennett, L., Frayer, D. T., Henderson, D., Lu, N., Masci, F., Pesenson, M., Rebull, L., Rho, J., Keene, J., Stolovy, S., Wachter, S., Wheaton, W., Werner, M. W., Richards, P. L. 2004. The Multiband Imaging Photometer for *Spitzer* (MIPS). *Astrophysical Journal Supplement Series* 154, 25-29.

Spitzer, L. Jr. 1978. *Physical Processes in the Interstellar Medium* (Wiley, New York)

Stanimirovic, S., Bolatto, A. D., Sandstrom, K., Leroy, A. K., Simon, J. D., Gaensler, B. M., Shah, R. Y., Jackson, J. M. 2005. *Spitzer* Space Telescope Detection of the Young Supernova Remnant 1E 0102.2-7219. *Astrophysical Journal* 632, L103-106.

Su, Y., & Chen, Y. 2005. A Narrow Band *Chandra* X-ray Analysis of SNR 3C 391. *Chinese Journal of Astronomy and Astrophysics* 5, 412-418.

Tappe, A., Rho, J., Reach, W. T. 2006. Shock processing of interstellar dust and polycyclic aromatic hydrocarbons in the supernova remnant N132D. *astro-ph/0609133*.

Wang, Z. R., Seward, F. D. 1984. X-rays from the SNR 3C 391. *Astrophysical Journal* 279, 705-707.

Werner, M. W., Roellig, T. L., Low, F. J., Rieke, G. H., Rieke, M., Hoffmann, W. F., Young, E., Houck, J. R., Brandl, B., Fazio, G. G., Hora, J. L., Gehrz, R. D., Helou, G., Soifer, B. T., Stauffer, J., Keene, J., Eisenhardt, P., Gallagher, D., Gautier, T. N., Irace, W., Lawrence, C. R., Simmons, L., Van Cleve, J. E., Jura, M., Wright, E. L., Cruikshank, D. P. 2004. The *Spitzer* Space Telescope Mission. *Astrophysical Journal Supplement Series* 154, 1-9.

Wilner, D. J., Reynolds, S. P., Moffett, D. A. 1998. CO observations toward the supernova remnant 3C 391. *Astronomical Journal* 115, 247-251.

Yusef-Zadeh, F., Wardle, M., Rho, J., & Sakano, M. 2003. OH (1720 MHz) Masers and Mixed-Morphology Supernova Remnants. *Astrophysical Journal* 585, 319-323.